Continuous versus discrete for interacting carbon nanostructures

2007 J. Phys. A: Math. Theor. 40 3851

(http://iopscience.iop.org/1751-8121/40/14/008)

IOP PUBLISHING JOURNAL OF PHYSICS A: MATHEMATICAL AND THEORETICAL

J. Phys. A: Math. Theor. **40** (2007) 3851–3868 doi:10.1088/1751-8113/40/14/008

Continuous versus discrete for interacting carbon nanostructures

Tamsyn A Hilder and James M Hill

Nanomechanics Group, School of Mathematics and Applied Statistics,
University of Wollongong, NSW 2522, Australia

E-mail: tah429@uow.edu.au and jhill@uow.edu.au

Received 12 December 2006, in final form 22 February 2007
Published 20 March 2007
Online at stacks.iop.org/JPhysA/40/3851

Abstract

Intermolecular forces between two interacting nanostructures can be obtained by either summing over all the individual atomic interactions or by using a continuum or continuous approach, where the number of atoms situated at discrete locations is averaged over the surface of each molecule. This paper aims to undertake a limited comparison of the continuum approach, the discrete atom–atom formulation and a hybrid discrete-continuum formulation for a range of molecular interactions involving a carbon nanotube, including interactions with another carbon nanotube and the fullerenes C_{60}, C_{70} and C_{80}. In the hybrid approach only one of the interacting molecules is discretized and the other is considered to be continuous. The hybrid discrete-continuum formulation would enable non-regular shaped molecules to be described, particularly useful for drug delivery systems which employ carbon nanotubes as carriers. The present investigation is important to obtain a rough estimate of the anticipated percentage errors which may occur between the various approaches in any specific application. Although our investigation is by no means comprehensive, overall we show that typically the interaction energies for these three approaches differ on average by at most 10% and the forces by 5%, with the exception of the C_{80} fullerene. For the C_{80} fullerene, while the intermolecular forces and the suction energies are in reasonable overall agreement, the point-wise energies can be significantly different. This may in part be due to differences in modelling the geometry of the C_{80} fullerene, but also the suction energies involve integrals of the energy, and therefore any errors or discrepancies in the point-wise energy tend to be smoothed out to give reasonable overall agreement for the former quantities.

PACS numbers: 81.07.De, 81.07.Nb, 81.05.Tp

(Some figures in this article are in colour only in the electronic version)

1. Introduction

Given the size and spatial distribution of atoms on a molecule the determination of the intermolecular forces between two interacting molecules is difficult to obtain analytically. The standard approach is to smear the atoms over the surface of each molecule by dividing the number of atoms by the surface area of each molecule, which is usually referred to as the continuum or continuous approximation. The question arises as to how the latter approach compares to the corresponding result obtained from a discrete atom–atom formulation and a hybrid discrete-continuum approach. The continuum approach is an important approximation and the purpose here is to investigate the discrepancies between the three techniques and if possible to arrive at a working estimate of the likely percentage difference that might be anticipated in any specific application.

Girifalco *et al* [1] state that

> "from a physical point of view the discrete atom–atom model is not necessarily preferable to the continuum model. The discrete model assumes that each atom is the centre of a spherically symmetric electron distribution while the continuum model assumes that the electron distribution is uniform over the surface. Both of these assumptions are incorrect and a case can even be made that the continuum model is closer to reality than a set of discrete Lennard–Jones centres."

One such example is a C_{60} fullerene, in which the molecule rotates freely at high temperatures so that the continuum distribution averages out the effect. Qian *et al* [2] suggest that the continuum approach is more accurate for the case where the

> "C nuclei do not lie exactly in the centre of the electron distribution, as is the case for carbon nanotubes."

However, one of the constraints of the continuum approach is that the shape of the molecule must be reasonably well defined so as to evaluate the integral analytically [2] and therefore the continuum approach is mostly applicable to highly symmetrical structures. Hodak and Girifalco [3] point out that the continuum approach ignores the effect of chirality and that nanotubes are only characterized by their diameters. The effect of chirality may be incorporated into other more sophisticated continuum mechanical theories, usually indirectly through the elastic moduli, such as in [4–6]. The continuum or continuous approximation has been successfully applied to a number of systems, including C_{60}-nanotube [1, 3, 7, 8], C_{60}–C_{60} [9] and nanotube–nanotube [1, 10, 11]. For the graphite-based and C_{60}-based potentials, Girifalco *et al* [1] state that calculations using the continuum and discrete approximations give similar results, such that the difference between equilibrium distances for the atom–atom interactions is less than 2%. Since Girifalco *et al* [1] provide very few details, the question arises as to the agreement for other fundamental quantities such as energy and force.

The aim of this paper is to further investigate such discrepancies and attempt to determine an average percentage difference for the interaction energies and forces for a range of geometric nanostructures. We compare the continuum approximation to both a discrete atom–atom formulation and a hybrid discrete-continuum formulation. In the latter approach one molecule is modelled discretely and the other is modelled using the continuum approximation. Motivated by the recent proposed use of nanotechnology in drug delivery, the hybrid method may be particularly applicable to non-regular shaped molecules, such as a particular drug, which might be modelled by the discrete approach, while the drug carrier as continuous. The interaction of the discrete modelled molecule with a continuum modelled carbon nanostructure, such as a carbon nanotube, is evaluated using the Lennard–Jones potential, which is the widely adopted

form for the interatomic potential of non-bonded and non-polar molecules. We assume that for the continuum approximation there is a uniform surface density of atoms, which is obtained simply by dividing the number of atoms by the surface area of the nanostructure. We show that typically the interaction energies for these three approaches differ on average by at most 10% while the forces differ by at most 5%, with the exception of the C_{80} fullerene.

In section 2, we outline the general approach together with the Lennard–Jones interatomic potential which is used in the three methods. Following this we model a single atom interacting with a carbon nanotube, and the nanotube is modelled both by continuum and discrete formulations for comparison. In the final sections of the paper we compare a number of particular systems arising from previous research including the interaction of C_{60}-nanotube [7], C_{70}-nanotube [12], C_{80}-nanotube [12] and nanotube–nanotube [11], and we use the hybrid discrete-continuum approach described in section 2. Certain mathematical details relating to the evaluation of integrals in terms of various hypergeometric functions and elliptic integrals are presented in appendices A and B.

2. Atomic interaction potentials

The non-bonded interaction energy, using the discrete formulation, is obtained by a summation of the interaction energy between each atom pair, thus

$$E = \sum_i \sum_j \upsilon(\rho_{ij}), \tag{1}$$

where $\upsilon(\rho_{ij})$ is the potential function for atoms i and j located a distance ρ_{ij} apart on two distinct molecular structures. We assume that each atom on the two molecules is well defined by a coordinate position. Following conventional practice, in the continuum approximation the atoms are assumed to be uniformly distributed over the surface of the molecule, and the double summation in (1) is therefore replaced by a double integral over the surface of each molecule, thus

$$E = \eta_1 \eta_2 \iint \upsilon(\rho)\, \mathrm{d}\Sigma_1\, \mathrm{d}\Sigma_2, \tag{2}$$

where η_1 and η_2 represent the mean surface density of the carbon atoms on the two interacting molecules, and now ρ represents the distance between two typical surface elements $\mathrm{d}\Sigma_1$ and $\mathrm{d}\Sigma_2$ located on the two interacting molecules. In this paper, we also examine a hybrid discrete-continuum model formulation, which is represented by elements of both (1) and (2), thus

$$E = \sum_i \eta_1 \int \upsilon(\rho_i)\, \mathrm{d}\Sigma_1, \tag{3}$$

which can be considered equivalent to either a double summation or a double integral. Table 1 provides the numerical values for the various constants used throughout the paper and we note that the mean surface density of the nanotube is always assumed to be equal to that of graphene. We comment that with E representing the total interaction energy, the various force components are determined by the negative gradient of E.

There are two major functional forms used in empirical models: the inverse power model and the Morse function model [8, 13]. In this investigation the so-called Lennard–Jones inverse power model is adopted and is given by

$$\upsilon(\rho) = 4\epsilon \left[-\left(\frac{\sigma}{\rho}\right)^6 + \left(\frac{\sigma}{\rho}\right)^{12} \right],$$

Table 1. Numerical values of constants.

Radius of C_{60}	3.55 Å
Radius[a] of (10, 10)	6.78 Å
Radius[a] of (16, 16)	10.856 Å
Radius[a] of (20, 20)	13.56 Å
Carbon–carbon bond length	$\sigma = 1.42$ Å
Mean surface density of graphene	$\eta_g = 4\sqrt{3}/(9\sigma^2)$ atoms Å^{-2}

[a] [14, p 885].

Table 2. Lennard–Jones constants for graphitic systems[a].

	A (eV×Å^6)	B (eV×Å^{12})	Model used
C–C[b]	19.97	34.81×10^3	C–CNT
Graphene–graphene	15.2	24.1×10^3	CNT–CNT
C_{60}–graphene	17.4	29.0×10^3	C_{60}–CNT, C_{80}–CNT

[a] [1].
[b] [9].

which is believed to apply to non-bonded and non-polar atomic interactions, where ϵ is the well depth, σ is the equilibrium distance and ρ is the distance between two atoms. Alternatively this may be written as

$$v(\rho) = -A\rho^{-6} + B\rho^{-12}, \tag{4}$$

where A and B are referred to as the attractive and repulsive constants, respectively. The equilibrium distance, ρ_0 between an atom pair is given by $\rho_0 = (2B/A)^{1/6}$. Table 2 outlines numerical values of the Lennard–Jones constants for the graphitic systems studied in this paper.

3. Carbon atom and a carbon nanotube

In this section, we evaluate the interaction between a single carbon atom and a carbon nanotube, first using the continuum approach followed by the discrete atom–atom formulation in which the carbon nanotube surface is completely discretized. With a rectangular Cartesian coordinate system at the tube centre, the distance between a single carbon atom and a typical atom of the carbon nanotube at $(a\cos\theta, a\sin\theta, z)$ is $\rho^2 = a^2 + (z - Z)^2$, where Z is the distance between the centre of the carbon nanotube and a single carbon atom assumed located on the axis of the nanotube and a is the radius of the carbon nanotube, and we use a (10, 10) configuration as given in table 1. Following Cox *et al* [7] the interaction energy between a single carbon atom and a carbon nanotube in the continuum approach is given by

$$E = 2\pi\eta a(-AI_6 + BI_{12}),$$

where I_n is equal to

$$I_n = \frac{1}{a^{2n-1}}\left[\frac{L-Z}{[a^2+(L-Z)^2]^{1/2}}F\left(\frac{3}{2}-n,\frac{1}{2};\frac{3}{2};\frac{(L-Z)^2}{a^2+(L-Z)^2}\right)\right.$$
$$\left. + \frac{L+Z}{[a^2+(L+Z)^2]^{1/2}}F\left(\frac{3}{2}-n,\frac{1}{2};\frac{3}{2};\frac{(L+Z)^2}{a^2+(L+Z)^2}\right)\right],$$

and $F(a, b; c; z)$ is the ordinary hypergeometric function [15], L is the half-length of the nanotube, and η is taken to be the surface density of graphene as given in table 1. In this paper,

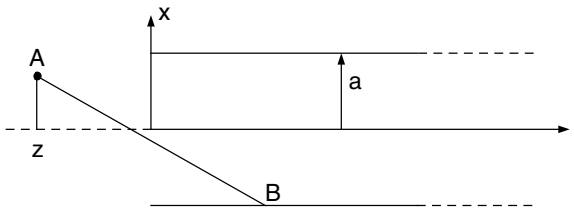

Figure 1. General offset atom and a carbon nanotube.

we require a finite length of nanotube in order to discretize the nanotube in the subsequent discrete atom–atom formulation. Consequently the integrals I_n have a different derivation in this paper from similar results in [7] and accordingly the details for the derivation required here are given in appendix A.

The interaction energy between a single carbon atom and the carbon nanotube in its discretized form is given by

$$E = \sum_{\gamma=1}^{N_c} \left(-A\rho_\gamma^{-3} + B\rho_\gamma^{-6}\right),$$

where N_c is the total number of atoms on the carbon nanotube and ρ_γ is the distance between the single carbon atom and a typical atom on the surface of the nanotube. The position of each atom on the carbon nanotube is found using simple trigonometry and application of the unit cell length for a carbon nanotube [14]. Using the algebraic package MAPLE we may plot the interaction energies corresponding to the two models. The carbon nanotube is taken to be 246 Å in length, which is equivalent to 4000 atoms in the discretized model. The attractive and repulsive constants, A and B, respectively are taken to be those of C–C, with values as given in table 2. We find that the overall trends agree for the two cases and that there is a 0.08% discrepancy between the minimum energies and 1.7% between the peak forces.

4. Further examples

In this section, we evaluate the hybrid discrete-continuum formulation in which one interacting body is discretized. We compare this to previously evaluated example problems for which the interaction potentials have been previously evaluated in the literature using the continuum approach. In the modelling of drug delivery systems, which employ carbon nanotubes as carriers, we would like to employ both discrete and continuum approaches to approximate the interaction energy for a drug molecule, which comprises various components including a number of isolated atoms. With this in mind the hybrid discrete-continuum approach enables the modelling of non-regular shaped molecules, such as drugs, and incorporates the time-saving advantage of leaving the carbon nanotube continuous. The aim here is to attempt to formulate a working estimate of the anticipated relative errors involved using this approach.

A general method is developed that can be used to model any shaped molecule. We define an offset atom at a distance z from the end of the carbon nanotube and at a radius ϵ from the axis of the carbon nanotube. It is assumed that the centre of mass of the entering molecule is located on the axis of the nanotube. With a cylindrical polar coordinate system (r, θ, z) at the tube centre, the offset atom is located at $A(\epsilon, 0, z)$ and a typical point on the nanotube is defined by $B(a\cos\theta, a\sin\theta, \xi)$ and we are assuming a semi-infinite tube, illustrated in figure 1.

The distance between the offset atom A and a typical point on the nanotube B is given by

$$\begin{aligned}\rho^2 &= (x_2 - x_1)^2 + (y_2 - y_1)^2 + (z_2 - z_1)^2 \\ &= (a+\epsilon)^2 - 4a\epsilon\cos^2(\theta/2) + (\xi - z)^2. \end{aligned} \tag{5}$$

Substituting (5) into (3) and (4), we obtain the energy of one offset atom interacting with the carbon nanotube, thus

$$E = \eta a \sum_{\gamma=1}^{N_a} \int_0^{\infty} \int_{-\pi}^{\pi} \left(\frac{-A}{[(a+\epsilon_\gamma)^2 + (\xi - z_\gamma)^2 - 4a\epsilon_\gamma \cos^2(\theta/2)]^3} + \frac{B}{[(a+\epsilon_\gamma)^2 + (\xi - z_\gamma)^2 - 4a\epsilon_\gamma \cos^2(\theta/2)]^6} \right) \mathrm{d}\theta \, \mathrm{d}\xi,$$

where η is the surface density of carbon atoms on the carbon nanotube as given in table 1, a is the radius of the nanotube and N_a is the number of atoms in the molecule. Given the symmetry of the problem we are principally only interested in the axial force, therefore on noting that $F = -\mathrm{d}E/\mathrm{d}z$ and evaluating the θ integration we obtain an interaction force given by

$$F = 2\pi\eta a \sum_{\gamma=1}^{N_a} \left[\frac{A}{\alpha_1^6} F\left(3, 1/2; 1; 1 - \alpha_2^2/\alpha_1^2\right) - \frac{B}{\alpha_1^{12}} F\left(6, 1/2; 1; 1 - \alpha_2^2/\alpha_1^2\right) \right], \tag{6}$$

where $\alpha_1^2 = (a+\epsilon_\gamma)^2 + (\xi - z_\gamma)^2$, $\alpha_2^2 = (a-\epsilon_\gamma)^2 + (\xi - z_\gamma)^2$ and details are given in appendix B. Note that again $F(a, b; c; x)$ denotes the ordinary hypergeometric function [15]. The interaction energy may be obtained by further integration with respect to ξ, thus

$$E = 2\pi\eta a \sum_{\gamma=1}^{N_a} \left[-A\left(\frac{1}{4}J_{3,3} + \frac{3}{8}(J_{1,5} + J_{5,1})\right) + B\left(\frac{63}{256}(J_{1,11} + J_{11,1}) + \frac{35}{256}(J_{3,9} + J_{9,3}) + \frac{30}{256}(J_{5,7} + J_{7,5})\right)\right]. \tag{7}$$

In terms of Appell's hypergeometric functions [16], $J_{m,n}$ is given by

$$J_{m,n} = \frac{\left[(a+\epsilon_\gamma)^2 + z_\gamma^2\right]^{-M}}{2} \frac{\Gamma(M)}{\Gamma(N)} F_1\left(M; \frac{n}{2}, \frac{1}{2}; N; (1-v^2)t_1, t_1\right),$$

where $M = (m+n-1)/2$, $N = (m+n+1)/2$, $v = (a-\epsilon_\gamma)/(a+\epsilon_\gamma)$, $t_1 = (a+\epsilon_\gamma)^2/\left[(a+\epsilon_\gamma)^2 + z_\gamma^2\right]$, and $F_1(a; b, b_1; c; x, y)$ is an Appell hypergeometric function. In terms of elliptic functions [17] we have

$$J_{i,j} = g\left[\frac{1}{\alpha^{2(i+j)}} \int_0^{\mathrm{tn}^{-1}\infty} \mathrm{sn}^{2i}u \, \mathrm{sd}^{2j}u \, \mathrm{d}u + \frac{1}{\alpha^{2i}\beta^{2j}} \int_0^{\mathrm{tn}^{-1}(z_\gamma/\beta)} \mathrm{c}\,\mathrm{d}^{2i}u \, \mathrm{cn}^{2j}u \, \mathrm{d}u\right],$$

where $i = (m-1)/2$, $j = (n-1)/2$, $\alpha = a + \epsilon_\gamma$, $\beta = a - \epsilon_\gamma$, $g = 1/\alpha$, and $\mathrm{tn}^{-1}(y, k) = \mathrm{sn}^{-1}(\sqrt{y^2/(1+y^2)}, k)$. We note that this is valid when $z_\gamma \geqslant 0$, and for the case when $z_\gamma \leqslant 0$ we have a subtraction rather than an addition of the two terms. Further details for both techniques are given in appendix B. We may use these offset atom formulae to determine both the force and energy for any shaped molecule, such as those presented in the following sub-sections.

4.1. Interaction of C_{60} fullerene with a carbon nanotube

Cox *et al* [7] and others [1, 3, 8] study the problem of the interaction of a carbon nanotube and a C_{60} fullerene. Here we compare the hybrid discrete-continuous model in which the C_{60}

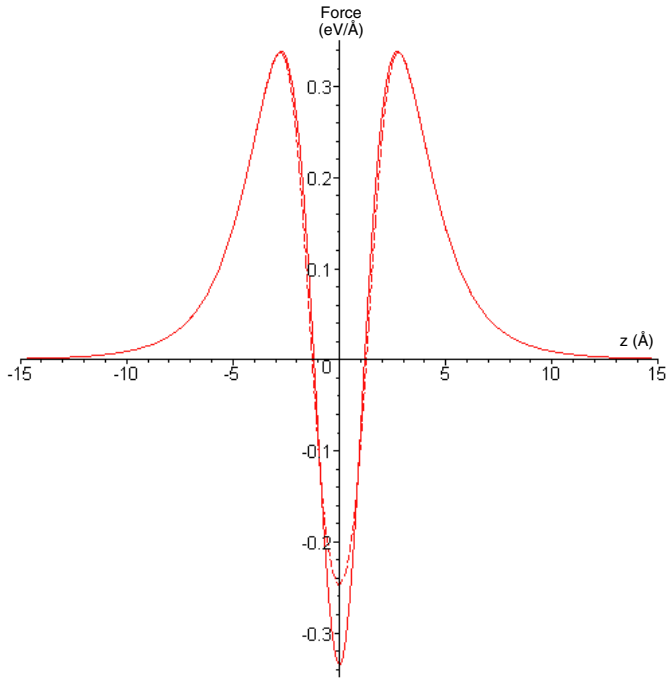

Figure 2. C_{60} force ($a = 6.4$ Å) for both hybrid discrete/continous (dash) and continuous (solid).

molecule is completely discretized, with that of the continuum approach as described by Cox *et al* [7].

We assume that the C_{60} fullerene is located on the central axis of the nanotube and there is no rotation. We note that Cox *et al* [7] find that for the (10, 10) configuration the buckyball's minimum energy position is on the central axis and as a result this is assumed here. Each individual atom in the fullerene (60 in total) is defined in terms of the Cartesian coordinates (x_1, x_2, x_3), which may be transformed into an ϵ and z position, thus

$$\epsilon = \sqrt{x_1^2 + x_2^2}, \qquad z = Z + x_3,$$

where Z is the distance between the centre of mass of the fullerene and the end of the carbon nanotube, since we assume a semi-infinite tube. The radius of the C_{60} fullerene is as given in table 1.

The force and energy of each atom in the fullerene are then evaluated by direct substitution of the atom position into the corresponding formulae (6) and (7), respectively. The resulting force and energy of the entire C_{60} fullerene with the carbon nanotube is then a summation over each atom, thus the total energy is given by $E = \sum_{\gamma=1}^{N_a} E(x_1, x_2, x_3)_\gamma$, where there are N_a atoms in the molecule, in the case of the C_{60} fullerene $N_a = 60$. Again using the algebraic package MAPLE we obtain plots for the force and energy.

We observe that the energy has the same trend in both the continuum and hybrid discrete-continuum methods. In fact, the two techniques provide identical plots with the exception of the maximum peak value which differ by at most 7%. The overall trends for the forces are also consistent between the two methods. However, there are discrepancies between the maximum and minimum peak values, illustrated in figure 2 for a nanotube radius $a = 6.4$ Å which represents the worst case. The average percentage difference of the two approaches for

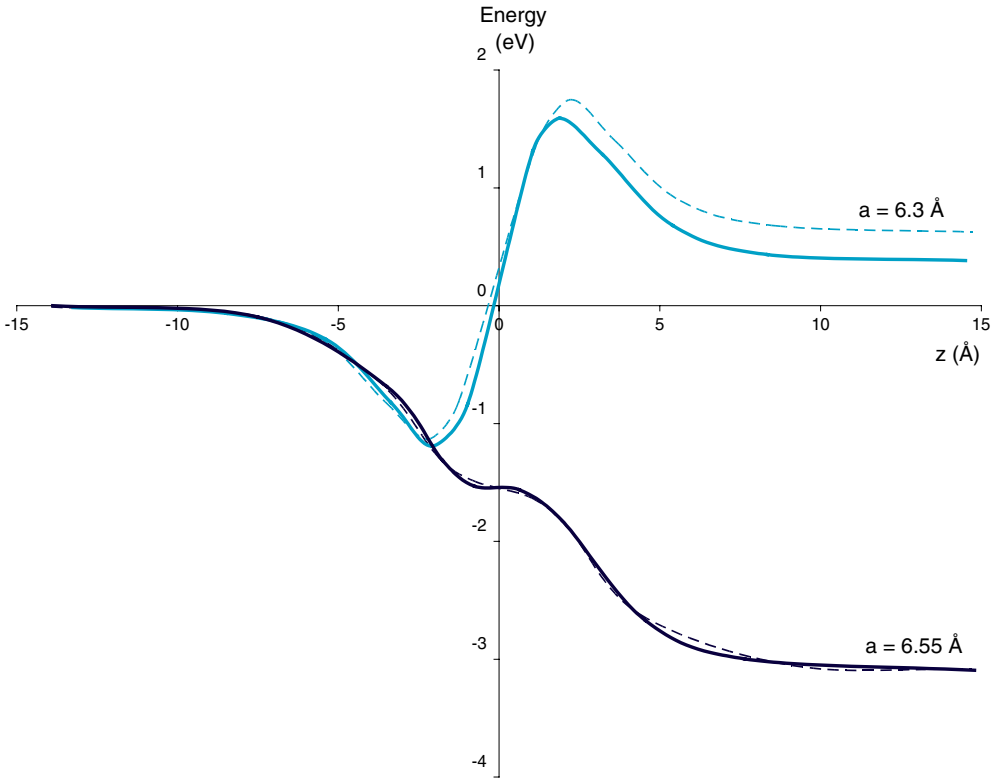

Figure 3. C_{70} energy for hybrid discrete-continuous (dash) and continuous (solid).

the three different carbon nanotube radii are 3.9% when $a = 6.4$ Å, 1.3% when $a = 6.509$ Å and 0.45% when $a = 6.784$ Å. We observe that for both the energy and force, as the nanotube radius decreases the average percentage difference increases.

4.2. Interaction of C_{70} and C_{80} fullerenes with a carbon nanotube

In this section, we examine the C_{70} and C_{80} fullerenes, comparing the hybrid discrete-continuum formulation to the continuum approach as presented by Cox *et al* [12]. It is important to note that the two approaches represent the fullerenes in a different way geometrically and therefore care must be taken when comparing the two results. For the case of the hybrid discrete-continuum formulation atom positions are defined by considering the C_{70} and C_{80} fullerenes as a cylinder of length 1.23 Å and 2.46 Å, respectively, capped at either end by a semi-spherical buckyball or C_{60} fullerene. Again, each atom has an ϵ and z position and the total force and energy are a sum of these individual results. The fullerenes presented continuously in Cox *et al* [12] are represented by perfect spheroidal surfaces and therefore are somewhat different in geometry to those fullerenes presented here. The C_{70} fullerene is closest in geometric shape to the spheroid and subsequently the results are closer for the C_{70}.

4.2.1. C_{70} fullerene. The C_{70} fullerene can be thought of as one row of carbon atoms centred on a cylindrical tube between two semi-spherical buckyball caps. As shown in figure 3 the

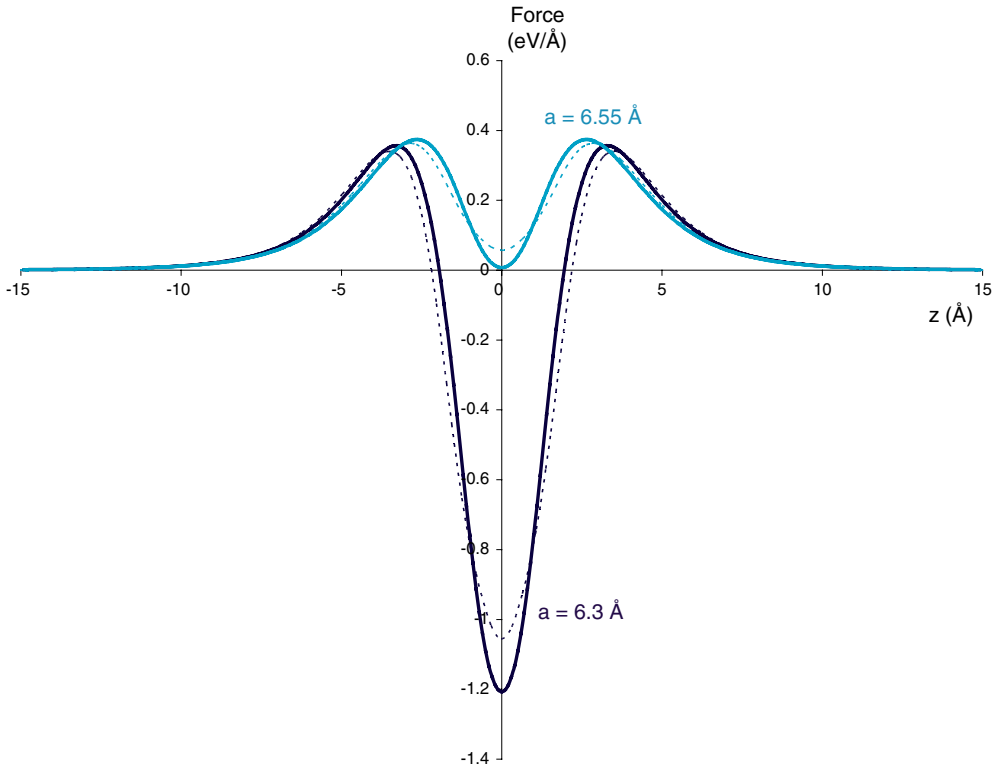

Figure 4. C_{70} force for hybrid discrete-continuous (dash) and continuous (solid).

overall trend is consistent between the two models but the magnitudes are somewhat different. For example for a nanotube radius $a = 6.3$ Å there is a 9.4% difference at the peak value. A comparison of the forces between the two models is shown in figure 4. Again the overall trend is consistent, the average percentage difference varies from 3% for $a = 6.55$ Å to 3.5% for $a = 6.3$ Å. Again, for both the energy and force, as the nanotube radius a decreases the average percentage difference increases.

4.2.2. C_{80} fullerene. The C_{80} fullerene can be thought of as one unit cell of a carbon nanotube, consisting of 20 carbon atoms and 10 hexagons, between two semi-spherical buckyball caps. Here the difference is more obvious between the two models, overall the trend is similar but there is a shift in the z position between the two models and the magnitudes are quite different, as shown in figure 5. For example for $a = 6.3$ Å the difference between peak values is 55%, again this difference decreases as the nanotube radius a increases, as shown in figure 5. This significant difference may be partly accounted for by the varying approach, in the continuum model the C_{80} is considered as a perfect spheroid, whereas here C_{80} is defined in the shape of a capsule. Figure 6 illustrates the forces for the two approaches. Here the trend differs slightly but the same acceptance conditions are predicted. The average percentage difference varies from 11.6% for $a = 6.54$ Å and 28.6% for $a = 6.3$ Å.

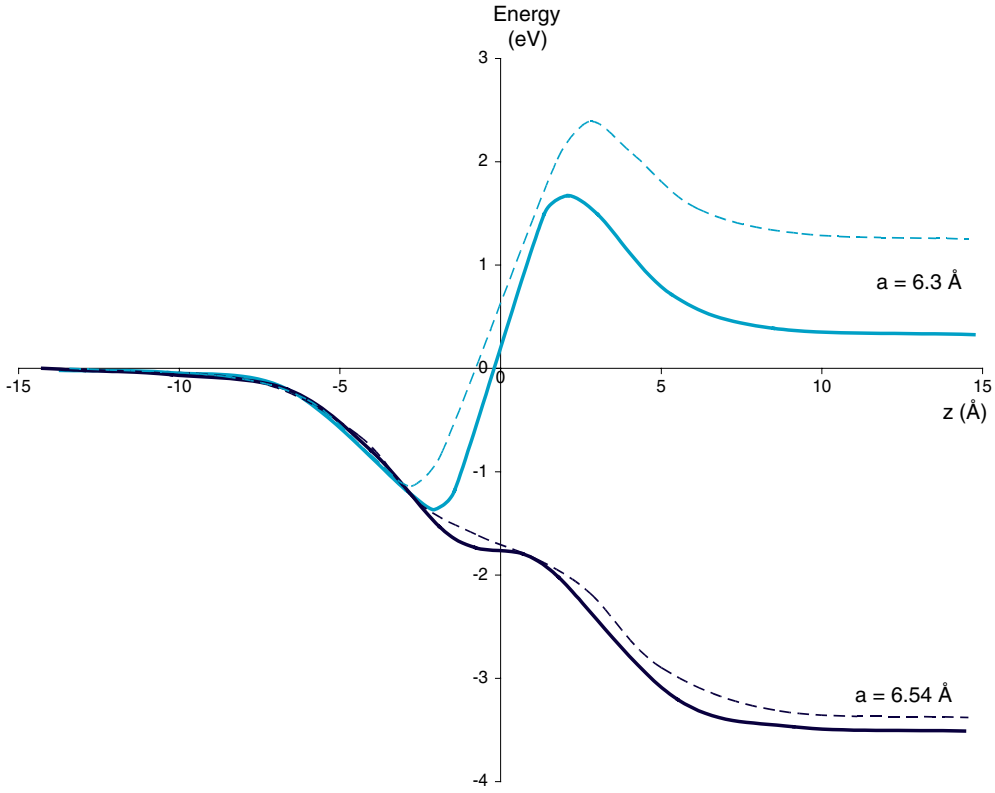

Figure 5. C_{80} energy for hybrid discrete-continuous (dash) and continuous (solid).

4.3. Suction energy

The suction energy is defined by Cox *et al* [18] as the energy that acts on the entering molecule so as to pull it into the interior of the carbon nanotube. It is defined as the integral

$$\int_{-\infty}^{\infty} F \, \mathrm{d}z = -\int_{-\infty}^{\infty} \frac{\mathrm{d}E}{\mathrm{d}z} \, \mathrm{d}z = E(-\infty) - E(\infty), \tag{8}$$

which is the work done that is transformed into kinetic energy. We have evaluated the suction energy to further investigate whether the hybrid discrete-continuous formulation predicts the same phenomenon as the continuous models. The comparison of suction energies is illustrated in figure 7 for the C_{60}, C_{70} and C_{80} fullerenes. Despite their obvious differences in magnitude for the point-wise energies the three fullerenes provide almost identical suction energies. In fact, the predicted nanotube radii that are energetically favourable to accept a particular fullerene are within 1% for the two approaches. Figure 5 illustrates that the discrepancy in approach is worst case for small radii. Figure 7 illustrates that at this small radii the curve has a steep gradient and as such a small change in radius may have a significant effect in energy. More specifically, from (8) the discrepancy in suction energy is influenced by the discrepancy in potential energy at $z = -\infty$ and $z = \infty$ for the two approaches. As shown in figure 5, the error at $-\infty$ is negligible but at ∞ is more significant, therefore the suction energy provides an

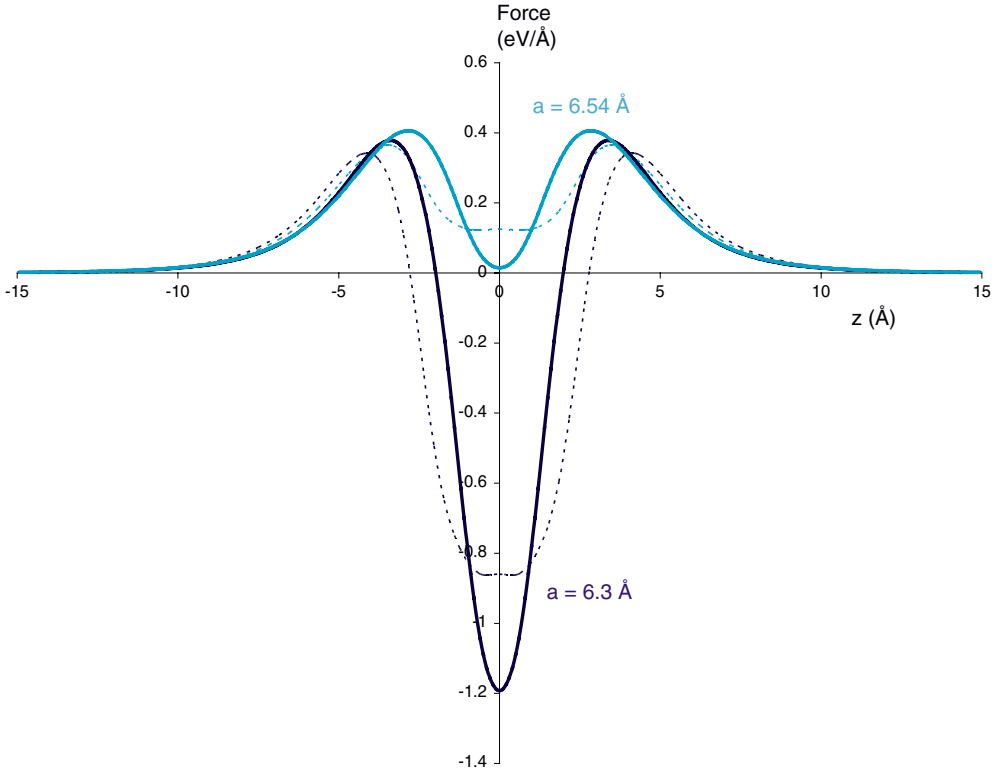

Figure 6. C_{80} force for hybrid discrete-continuous (dash) and continuous (solid).

Table 3. Double-walled carbon nanotube, hybrid discrete-continuous versus continuous.

	Energy (%)	Force (%)
(10, 10) and (16, 16)	0.93	0.12
(10, 10) and (20, 20)	0.9	0.01

averaged result and consequently provides a smaller discrepancy between the two approaches. Overall the two techniques provide very similar results.

4.4. Interaction of double-walled carbon nanotubes

Baowan and Hill [11] and others [1, 10] study the interaction of double-walled carbon nanotubes. Here we compare the continuum model of Baowan and Hill [11] to our hybrid discrete-continuous method in which the inner tube is discretized and the outer tube remains continuous. Note that the (10, 10) nanotube is always the discretized tube, and is equivalent to 4000 atoms. Again we use the offset atom formulae given by (6) and (7) for the force and energy, respectively and sum over all atoms. The general trend for both the force and energy curves are consistent between the two methods. As shown in table 3, where two configurations of double-walled nanotubes are investigated, the peak values differ by less than 1%.

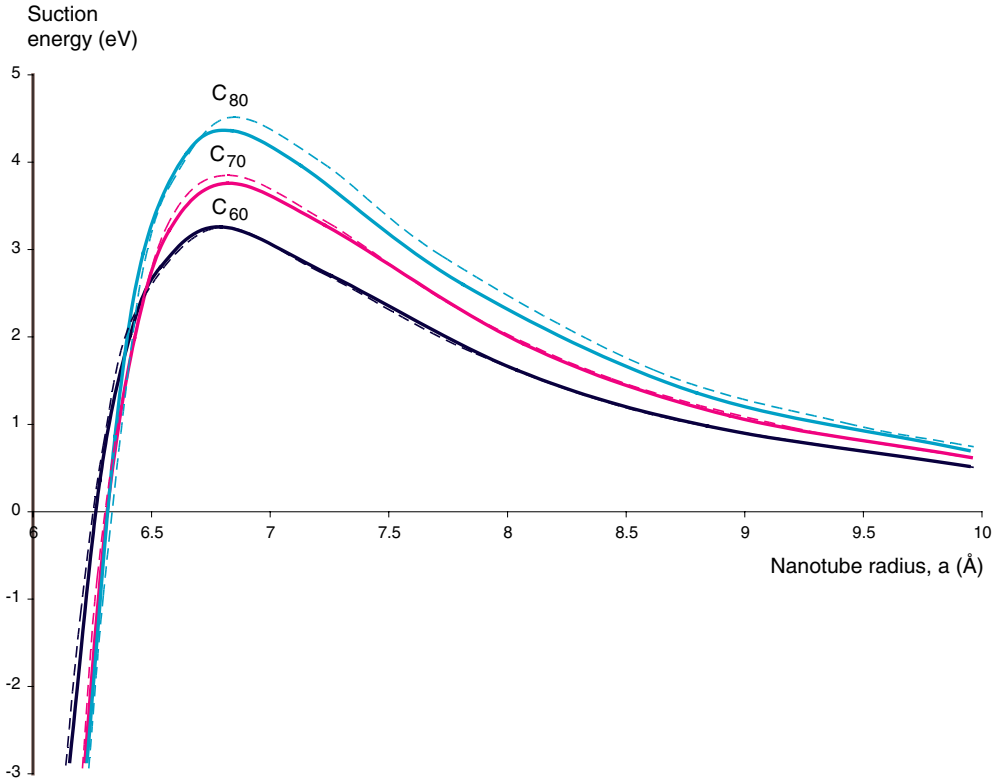

Figure 7. Suction energy for hybrid discrete-continuous (dash) and continuous (solid).

5. Conclusions

In order to calculate the atomic interaction energies for two interacting nanostructures, we can either sum over all the individual atomic interactions, or we can adopt a continuum approach using a smeared atomic density, or we can employ a hybrid discrete-continuum approach which utilizes both procedures. The latter approach might be especially useful for proposed drug delivery systems which use carbon nanotubes as carriers and there is need to determine whether or not a specific molecule is energetically favourable to be accepted into a specific carbon nanotube. The drug may be modelled by the discrete approach, or a combination of both the discrete and continuous approaches if necessary, while the carbon nanotube carrier would be modelled continuously.

In this paper, we find that the discrete atom–atom formulation has a similar trend and is within 2% of the continuum approach. Similarly, we find that the continuum approach and hybrid discrete-continuum approach are similar in both trend and magnitude. However, geometry (even though symmetric) appears to have a significant effect in causing a discrepancy between the two methods, in particular for the C_{70} and C_{80} fullerenes. However, although there are discrepancies, the same physical phenomenon is still predicted by both approaches. Typically the interaction energies for the three approaches differ by at most 10% and the forces by 5%, with the exception of the C_{80} fullerene. For the C_{80} fullerene, while the intermolecular forces and the suction energies are in reasonable overall agreement, the point-wise energies

Table 4. Overview of differences for particular geometries.

	Energy (%)	Force (%)
Atom–nanotube	0.08	1.7
C_{60}-nanotube	<5	<4
C_{70}-nanotube	<9.4	3–3.5
C_{80}-nanotube	<55	11–28
Nanotube–nanotube	<1	<1

can be significantly different. This may be because the suction energies involve integrals of the energy, and therefore any errors or discrepancies in the point-wise energy tend to be smoothed out to give reasonable overall agreement for the former quantities. The significant discrepancy shown between the two approaches for the C_{80} fullerene may in part be due to the difference in the modelling of the geometric shape. For this case the continuum model of the C_{80} fullerene is represented as a perfect ellipsoid while in the hybrid model it is represented as two caps and a cylinder. For both the energy and force for all fullerenes presented in this paper, the average percentage difference increases as the carbon nanotube radius a decreases. Table 4 provides an overview of the resulting differences between the various models studied in this paper.

Acknowledgments

The authors are grateful to the Australian Research Council for support through the Discovery Project Scheme and the University of Wollongong for a University Postgraduate Award. In particular, JMH is grateful to the Australian Research Council for provision of an Australian Professorial Fellowship. The authors especially wish to acknowledge their colleagues Barry Cox, Grant Cox, Ngamta Thamwattana and Duangkamon Baowan for many helpful comments and discussions.

Appendix A. Carbon atom and nanotube of finite length

The interaction energy is given by

$$E = \eta \int_0^{2\pi} \int_{-L}^{L} \left(\frac{-A}{\rho^6} + \frac{B}{\rho^{12}} \right) a \, \mathrm{d}z \, \mathrm{d}\theta = 2\pi a \eta \int_{-L}^{L} \left(\frac{-A}{\rho^6} + \frac{B}{\rho^{12}} \right) \mathrm{d}z,$$

where $\rho^2 = a^2 + (z - Z)^2$. We then have the integral

$$I_n = \int_{-L}^{L} \frac{\mathrm{d}z}{[a^2 + (z - Z)^2]^n} = \int_{-\omega_1}^{\omega_2} a^{1-2n} \sec^{2-2n} \omega \, \mathrm{d}\omega,$$

where we have made the substitution $z = Z + a \tan\omega$, $\omega_1 = \tan^{-1}[(L + Z)/a]$, $\omega_2 = \tan^{-1}[(L - Z)/a]$ and we are interested in the two values $n = 3$ and $n = 6$. On making the further substitution $t = \tan\omega$ we obtain

$$I_n = a^{1-2n} \int_{-t_1}^{t_2} \frac{\mathrm{d}t}{(t^2 + 1)^n} = a^{1-2n} \left[\int_0^{t_2} \frac{\mathrm{d}t}{(t^2 + 1)^n} + \int_0^{t_1} \frac{\mathrm{d}t}{(t^2 + 1)^n} \right],$$

where $t_1 = (L + Z)/a$ and $t_2 = (L - Z)/a$. We now make the substitution

$$x = t(1 + t^2)^{-1/2}, \qquad t = x(1 - x^2)^{-1/2}, \qquad \mathrm{d}t = \mathrm{d}x(1 - x^2)^{-3/2},$$

and we use the transformation $B(\beta, \gamma-\beta)F(\alpha, \beta; \gamma; z) = \int_0^1 t^{\beta-1}(1-t)^{\gamma-\beta-1}(1-tz)^{-\alpha}\,\mathrm{d}t$ from Gradshteyn and Ryzhik [15, p 995] to obtain the result in terms of ordinary hypergeometric functions, thus

$$I_n = a^{1-2n}\left[\frac{L-Z}{[a^2+(L-Z)^2]^{1/2}}F\left(\frac{3}{2}-n, \frac{1}{2}; \frac{3}{2}; \frac{(L-Z)^2}{a^2+(L-Z)^2}\right) + \frac{L+Z}{[a^2+(L+Z)^2]^{1/2}}F\left(\frac{3}{2}-n, \frac{1}{2}; \frac{3}{2}; \frac{(L+Z)^2}{a^2+(L+Z)^2}\right)\right].$$

Appendix B. Offset atom interaction energy

B.1. Evaluation of θ integration

We have the integral

$$E = \eta a \sum_\gamma \int_0^\infty \int_{-\pi}^{\pi} \left(\frac{-A}{[(a+\epsilon_\gamma)^2+(\xi-z_\gamma)^2-4a\epsilon_\gamma\cos^2(\theta/2)]^3} + \frac{B}{[(a+\epsilon_\gamma)^2+(\xi-z_\gamma)^2-4a\epsilon_\gamma\cos^2(\theta/2)]^6}\right)\mathrm{d}\theta\,\mathrm{d}\xi,$$

and on letting $\phi = \theta/2$ we obtain the general θ integration

$$I_n = 2\int_{-\pi/2}^{\pi/2} \frac{\mathrm{d}\phi}{\left[\alpha_1^2+\left(\alpha_2^2-\alpha_1^2\right)\cos^2\phi\right]^n},$$

where $\alpha_1^2 = (a+\epsilon_\gamma)^2+(\xi-z_\gamma)^2$, $\alpha_2^2 = (a-\epsilon_\gamma)^2+(\xi-z_\gamma)^2$, $\alpha_2^2-\alpha_1^2 = -4a\epsilon_\gamma$ and we are interested in the values $n=3$ and $n=6$. Given the symmetry of the integral and making the substitution $t = \cos^2\phi$ we obtain

$$I_n = 4\int_0^{\pi/2} \frac{\mathrm{d}\phi}{\left[\alpha_1^2+\left(\alpha_2^2-\alpha_1^2\right)\cos^2\phi\right]^n} = \frac{2}{\alpha_1^{2n}}\int_0^1 \frac{t^{-1/2}(1-t)^{-1/2}}{[1-(1-(\alpha_2/\alpha_1)^2)t]^n}\,\mathrm{d}t.$$

From Gradshteyn and Ryzhik [15, p 995] we use the relation

$$\int_0^1 t^{\beta-1}(1-t)^{\gamma-\beta-1}(1-tz)^{-\alpha}\,\mathrm{d}t = B(\beta, \gamma-\beta)F(\alpha, \beta; \gamma; z),$$

and obtain the integral in terms of the ordinary hypergeometric function, thus

$$I_n = \frac{2}{\alpha_1^{2n}}B\left(\frac{1}{2}, \frac{1}{2}\right)F\left(n, \frac{1}{2}; 1; 1-\left(\frac{\alpha_2}{\alpha_1}\right)^2\right) = \frac{2\pi}{\alpha_1^{2n}}F\left(n, \frac{1}{2}; 1; 1-\left(\frac{\alpha_2}{\alpha_1}\right)^2\right).$$

From Erdélyi *et al* [19, pp 64 and 69] it can be shown that the hypergeometric function given above is quadratic and degenerate, respectively. Using the transformation on page 69, $F(a, b; c; x) = (1-x)^{c-a-b}F(c-a, c-b; c; x)$, we obtain two degenerate functions for $n=3$ and $n=6$ given by

$$F(3, 1/2; 1; x) = \left(\frac{\alpha_1}{\alpha_2}\right)^5\left(1-x+\frac{3x^2}{8}\right),$$

$$F(6, 1/2; 1; x) = \left(\frac{\alpha_1}{\alpha_2}\right)^{11}\left(1-\frac{5x}{2}+\frac{15x^2}{4}-\frac{25x^3}{8}+\frac{175x^4}{128}-\frac{63x^5}{256}\right),$$

where $x = 1-(\alpha_2/\alpha_1)^2$. Expanding these results and substituting into the original interaction energy equation we obtain

$$E = 2\pi\eta a\left[-A\left(\frac{1}{4}J_{3,3}+\frac{3}{8}(J_{1,5}+J_{5,1})\right)\right.$$
$$\left.+B\left(\frac{63}{256}(J_{1,11}+J_{11,1})+\frac{35}{256}(J_{3,9}+J_{9,3})+\frac{30}{256}(J_{5,7}+J_{7,5})\right)\right],$$

where

$$J_{m,n} = \int_0^\infty \frac{\mathrm{d}\xi}{\alpha_1^m\alpha_2^n}. \tag{B.1}$$

B.2. Evaluation of ξ integration

We now evaluate the ξ integration given by (B.1) using both Appell's hypergeometric functions and elliptic functions. The integral is of the form

$$J_{m,n} = \int_0^\infty \frac{\mathrm{d}\xi}{[(a+\epsilon_\gamma)^2+(\xi-z_\gamma)^2]^p[(a-\epsilon_\gamma)^2+(\xi-z_\gamma)^2]^q},$$

where we let $m = 2p$ and $n = 2q$.

B.2.1. Appell's hypergeometric functions. On making the substitution $\xi - z_\gamma = (a+\epsilon_\gamma)\tan\omega$ we obtain

$$\begin{aligned}J_{2p,2q} &= \int_{\omega_1}^{\pi/2} \frac{(a+\epsilon_\gamma)\sec^2\omega\,\mathrm{d}\omega}{[(a+\epsilon_\gamma)^2+(a+\epsilon_\gamma)^2\tan^2\omega]^p[(a-\epsilon_\gamma)^2+(a+\epsilon_\gamma)^2\tan^2\omega]^q}\\ &= (a+\epsilon_\gamma)^{1-2p}\int_{\omega_1}^{\pi/2}\frac{(\cos^2\omega)^{p-1}\cos^{2q}\omega\,\mathrm{d}\omega}{[(a-\epsilon_\gamma)^2\cos^2\omega+(a+\epsilon_\gamma)^2\sin^2\omega]^q}\\ &= (a+\epsilon_\gamma)^{1-2p-2q}\int_{\omega_1}^{\pi/2}\frac{(\cos^2\omega)^{p+q-1}\,\mathrm{d}\omega}{[1-(1-v^2)\cos^2\omega]^q},\end{aligned}$$

where $\omega_1 = \tan^{-1}(-z_\gamma/(a+\epsilon_\gamma))$ and $v = (a-\epsilon_\gamma)/(a+\epsilon_\gamma)$. We now make the further substitutions $t = \cos^2\omega$ and $t = t_1 u$, thus

$$\begin{aligned}J_{2p,2q} &= \frac{(a+\epsilon_\gamma)^{1-2p-2q}}{2}\int_0^{t_1} t^{p+q-1}t^{-1/2}(1-t)^{-1/2}(1-(1-v^2)t)^{-q}\,\mathrm{d}t\\ &= \frac{\left[(a+\epsilon_\gamma)^2+z_\gamma^2\right]^{1/2-p-q}}{2}\int_0^1 u^{p+q-3/2}(1-t_1u)^{-1/2}[1-(1-v^2)t_1u]^{-q}\,\mathrm{d}u,\end{aligned}$$

where $t_1 = (a+\epsilon_\gamma)^2/\left[(a+\epsilon_\gamma)^2+z_\gamma^2\right]$. From Bailey [16, p 77] we use the relation

$$\int_0^1 u^{\alpha-1}(1-u)^{\gamma-\alpha-1}(1-ux)^{-\beta_1}(1-uy)^{-\beta_2}\,\mathrm{d}u$$
$$= \frac{\Gamma(\alpha)\Gamma(\gamma-\alpha)}{\Gamma(\gamma)}F_1(\alpha;\beta_1,\beta_2;\gamma;x,y),$$

and we write $J_{2p,2q}$ in terms of Appell's hypergeometric function of two variables, thus

$$J_{m,n} = \frac{\left[(a+\epsilon_\gamma)^2+z_\gamma^2\right]^{-M}}{2}\frac{\Gamma(M)}{\Gamma(N)}F_1\left(M;\frac{n}{2},\frac{1}{2};N;(1-v^2)t_1,t_1\right),$$

where $M = (m+n-1)/2$ and $N = (m+n+1)/2$.

B.2.2 Elliptic integrals. Alternatively we can evaluate the ξ integration using elliptic integrals. We write the integral in the form

$$\begin{aligned} J_{i,j} &= \int_{-z_\gamma}^{\infty} \frac{\mathrm{d}t}{[\alpha^2+t^2]^i[\beta^2+t^2]^j\sqrt{(\alpha^2+t^2)(\beta^2+t^2)}} \\ &= \int_{0}^{\infty} \frac{\mathrm{d}t}{[\alpha^2+t^2]^i[\beta^2+t^2]^j\sqrt{(\alpha^2+t^2)(\beta^2+t^2)}} \\ &\quad + \int_{0}^{z_\gamma} \frac{\mathrm{d}t}{[\alpha^2+t^2]^i[\beta^2+t^2]^j\sqrt{(\alpha^2+t^2)(\beta^2+t^2)}} \\ &= K_{i,j} + K^*_{i,j}, \end{aligned} \tag{B.2}$$

where $i = (m-1)/2$, $j = (n-1)/2$ and we have made the substitution $t = \xi - z_\gamma$ and let $\alpha = a + \epsilon_\gamma$, $\beta = a - \epsilon_\gamma$. We now evaluate the integrals $K_{i,j}$ with integration limits $[0, \infty]$ and $K^*_{i,j}$ with limits $[0, z_\gamma]$. Using Byrd and Friedman [17, p 62] we evaluate $K_{i,j}$, where

$$\mathrm{tn}^2 u = (\alpha/t)^2, \qquad k^2 = 1 - (\beta/\alpha)^2, \qquad g = 1/\alpha.$$

Using elliptic identities we obtain a relation between $\mathrm{d}u$ and $\mathrm{d}t$, thus $\mathrm{d}t = -[(\alpha^2+t^2)(\beta^2+t^2)]^{1/2}\,\mathrm{d}u/\alpha$, which on substituting into the original integral obtains

$$K_{i,j} = \frac{g}{\alpha^{2(i+j)}} \int_0^{u_1} \mathrm{sn}^{2i} u\, \mathrm{sd}^{2j} u\, \mathrm{d}u, \tag{B.3}$$

where $u_1 = \mathrm{tn}^{-1}\infty$ or $u_1 = \mathrm{sn}^{-1}(1, k)$. Similarly using Byrd and Friedman [17, p 61] we evaluate $K^*_{i,j}$, where

$$\mathrm{tn}^2 u = (t/\beta)^2, \qquad k^2 = 1 - (\beta/\alpha)^2, \qquad g = 1/\alpha.$$

Using the elliptic identities we again obtain a relation between $\mathrm{d}u$ and $\mathrm{d}t$, thus $\mathrm{d}t = [(\alpha^2+t^2)(\beta^2+t^2)]^{1/2}\,\mathrm{d}u/\alpha$, which on substituting into the original integral obtains

$$K^*_{i,j} = \frac{g}{\alpha^{2i}\beta^{2j}} \int_0^{u_1} \mathrm{c}\,\mathrm{d}^{2i} u\, \mathrm{cn}^{2j} u\, \mathrm{d}u, \tag{B.4}$$

where here we have $u_1 = \mathrm{tn}^{-1}(z_\gamma/\beta)$ and $z_\gamma \geqslant 0$. From Byrd and Friedman [17, p 209 (351.51)] we have the transformation

$$\int \frac{\mathrm{sn}^{2q} u\, \mathrm{cn}^{2r} u}{\mathrm{dn}^{2s} u}\,\mathrm{d}u = \frac{1}{k^{2(q+r)}} \sum_{\tau=0}^{q}\sum_{\mu=0}^{r} \frac{(-1)^{\tau+\mu+r}(1-k^2)^{2(r-\mu)} q!r!}{(q-\tau)!\tau!(r-\mu)!\mu!} I_{2(s-\tau-\mu)},$$

which can be used with the elliptic identities to simplify the original elliptic integrals (B.3) and (B.4), thus

$$K_{i,j} = \frac{g}{(k\alpha)^{2(i+j)}} \sum_{\mu=0}^{i+j} \frac{(-1)^\mu (i+j)!}{(i+j-\mu)!\mu!} I_{2(j-\mu)}\Big|_{u_1},$$

$$K^*_{i,j} = \frac{g}{\alpha^{2i}\beta^{2j}k^{2(i+j)}} \sum_{\mu=0}^{i+j} (1-k^2)^{i+j-\mu} \frac{(-1)^{\mu+i+j}(i+j)!}{(i+j-\mu)!\mu!} I_{2(i-\mu)}\Big|_{u_1^*},$$

where $u_1 = \mathrm{sn}^{-1}(1, k)$, $u_1^* = \mathrm{sn}^{-1}\left(z_\gamma \big/ \left(z_\gamma^2 + \beta^2\right)^{1/2}, k\right)$ and if $x \leqslant 0$ we note that $I_x = G_{|x|} = \int \mathrm{dn}^{|x|} u\,\mathrm{d}u$ since $\mathrm{nd}^{-x} u = \mathrm{dn}^x u$, alternatively if $x > 0$ we have $I_x = H_x = \int \mathrm{nd}^x u\,\mathrm{d}u$. The

value of $G_{|x|}$ and H_x can be evaluated using the recurrence formulae given on page 194 of Byrd and Friedman [17], thus

$$G_x = \int \mathrm{dn}^x u \, \mathrm{d}u, \qquad G_0 = u, \qquad G_2 = E(\varphi, k),$$

$$G_{2m+2} = \frac{k^2 \, \mathrm{dn}^{2m-1} u \, \mathrm{sn}u \, \mathrm{cn}u + (1-2m)(1-k^2)G_{2m-2} + 2m(2-k^2)G_{2m}}{2m+1},$$

$$H_x = \int \mathrm{nd}^x u \, \mathrm{d}u, \qquad H_0 = u, \qquad H_2 = \frac{1}{(1-k^2)}[E(\varphi, k) - k^2 \mathrm{sn}u \, \mathrm{cd}u],$$

$$H_{2m+2} = \frac{2m(2-k^2)H_{2m} + (1-2m)H_{2m-2} - k^2 \mathrm{sn}u \, \mathrm{cn}u \, \mathrm{nd}^{2m+1} u}{(2m+1)(1-k^2)}.$$

Note that when $z_\gamma < 0$ equation (B.2) becomes

$$\begin{aligned} J^*_{i,j} &= \int_0^\infty \frac{\mathrm{d}t}{[\alpha^2 + t^2]^i [\beta^2 + t^2]^j \sqrt{(\alpha^2 + t^2)(\beta^2 + t^2)}} \\ &\quad - \int_0^{-z_\gamma} \frac{\mathrm{d}t}{[\alpha^2 + t^2]^i [\beta^2 + t^2]^j \sqrt{(\alpha^2 + t^2)(\beta^2 + t^2)}} \\ &= K_{i,j} - K^*_{i,j}, \end{aligned}$$

and the elliptic integral method is still valid. The resulting interaction energy from the elliptic integration becomes

$$E = 2\pi\eta a \sum_\gamma \left[-A\left(\frac{1}{4}J_{1,1} + \frac{3}{8}(J_{0,2} + J_{2,0})\right) + B\left(\frac{63}{256}(J_{0,5} + J_{5,0}) + \frac{35}{256}(J_{1,4} + J_{4,1}) + \frac{30}{256}(J_{2,3} + J_{3,2})\right)\right].$$

References

[1] Girifalco L A, Hodak M and Lee R S 2000 Carbon nanotubes, buckyballs, ropes and a universal graphitic potential *Phys. Rev.* B **62** 104–110

[2] Qian D, Liu W K, Subramoney S and Ruoff R S 2003 Effect of the interlayer potential on mechanical deformation of multiwalled carbon nanotubes *J. Nanosci. Nanotech.* **3** 185–91

[3] Hodak M and Girifalco L A 2001 Fullerenes inside carbon nanotubes and multi-walled carbon nanotubes: optimum and maximum sizes *Chem. Phys. Lett.* **350** 405–11

[4] Leamy M J 2007 Bulk dynamic response modeling of carbon nanotubes using an intrinsic finite element formulation incorporating interatomic potentials *Int. J. Solids Struct.* **44** 874–94

[5] Arroyo M and Belytschko T 2004 Finite crystal elasticity of carbon nanotubes based on the exponential Cauchy–Born rule *Phys. Rev.* B **69** 115415

[6] Zhang P, Huang Y, Geubelle P H, Klein P A and Hwang K C 2002 The elastic modulus of single-walled carbon nanotubes: a continuum analysis incorporating interatomic potentials *Int. J. Solids Struct.* **39** 3893–906

[7] Cox B J, Thamwattana N and Hill J M 2007 Mechanics of atoms and fullerenes in single-walled carbon nanotubes: II. Oscillatory behaviour *Proc. R. Soc.* A **463** 477–94

[8] Qian D, Liu W K and Ruoff R S 2001 Mechanics of C_{60} in nanotubes *J. Phys. Chem.* B **105** 10753–8

[9] Girifalco L A 1992 Molecular properties of C_{60} in the gas and solid phases *J. Phys. Chem.* **96** 858–61

[10] Zheng Q, Liu J Z and Jiang Q 2002 Excess van der Waals interaction energy of a multiwalled carbon nanotube with an extruded core and the induced core oscillation *Phys. Rev.* B **65** 245409

[11] Baowan D and Hill J M 2007 Force distribution for double-walled carbon nanotubes and gigahertz oscillators *Z. Angew. Math. Phys.* **58** at press

[12] Cox B J, Thamwattana N and Hill J M 2007 Mechanics of spheroidal fullerenes and carbon nanotubes for drug and gene delivery *Q. J. Mech. Appl. Math.* **60** at press

[13] Wang Y, Tománek D and Bertsch G F 1991 Stiffness of solid composed of C_{60} clusters *Phys. Rev.* B **44** 6562–65

[14] Dresselhaus M S, Dresselhaus G and Saito R 1995 Physics of carbon nanotubes *Carbon* **33** 883–91

[15] Gradshteyn I S and Ryzhik I M 2000 *Table of Integrals, Series and Products* 6th edn (San Diego, USA: Academic)
[16] Bailey W N 1972 *Generalized Hypergeometric Series* (New York: Hafner Publishing)
[17] Byrd P F and Friedman M D 1971 *Handbook of Elliptic Integrals for Engineers and Scientists* 2nd edn (Berlin: Springer)
[18] Cox B J, Thamwattana N and Hill J M 2007 Mechanics of atoms and fullerenes in single-walled carbon nanotubes: I. Acceptance and suction energies *Proc. R. Soc.* A **463** 461–76
[19] Erdélyi A, Magnus W, Oberhettinger F and Tricomi F G 1953 *Higher Transcendental Functions* vol 1 (New York: McGraw-Hill)